Nuclear Instruments and Methods in Physics Research A 1069 (2024) 169944

Contents lists available at ScienceDirect

Nuclear Inst. and Methods in Physics Research, A

journal homepage: www.elsevier.com/locate/nima

Full Length Article

# LSTAR — An isobar separator for expanding radioactive ion beam production at the Cyclotron Institute, Texas A&M University

G.P.A Berg [c,*], D. Melconian [a,b], M. Couder [c], M. Brodeur [c], V.E. Iacob [a], J. Klimo [a], P.D. Shidling [a]

[a] Cyclotron Institute, Texas A&M University, College Station, 77843-3366, TX, USA
[b] Department of Physics & Astronomy, Texas A&M University, College Station, 77843-4242, TX, USA
[c] Department of Physics & Astronomy, University of Notre Dame, Notre Dame, 46556, IN, USA

ARTICLE INFO

*Keywords:*
Magnetic instruments and components
Charged-particle spectrometers
Electric and magnetic
Beam optics

ABSTRACT

A new isobar separator, LSTAR (Light-ion guide Separator for Texas A&M's Radioactive ion beams), has been designed to purify the exotic beams produced by a He-driven light-ion guide (He-LIG) system at Texas A&M University, primarily for the TAMUTRAP experiment. The main purpose of TAMUTRAP is to probe for physics beyond the standard model by searching for possible scalar or tensor currents in the weak interaction using nuclear $\beta$ decay. The proton-rich isotopes of interest for this program will be produced at low yields, requiring efficient reduction of contaminant species to avoid overloading of TAMUTRAP's radiofrequency quadrupole cooler-buncher. The layout, ion-optics, and specifications of LSTAR will be presented.

## 1. Introduction

The goal of TAMUTRAP, a new facility under development at the Cyclotron Institute at Texas A&M University [1], is to probe for physics beyond the standard model by searching for possible scalar or tensor currents in the weak interaction in nuclear $\beta$ decay [2,3].

TAMUTRAP has been built as a system which is uniquely suited to measure observables of $\beta$-delayed proton decays very precisely. Once radioactive ion beams from the Cyclotron Institute's K150 cyclotron using the IGISOL (Ion Guide Isotope Separator On-Line) technique [4] are available for TAMUTRAP, we will be able to measure correlation parameters and comparative half-lives in a number of neutron-deficient nuclei for testing the charged electroweak sector of the standard model. In order to attain the sensitivities necessary to impact the field, these correlation and half-life measurements must achieve $\lesssim 0.1\%$ precision [3]. The TAMUTRAP facility will reach this goal by utilizing the open geometry and ideal source conditions of ions confined in the world's biggest cylindrical Penning trap [1].

The Penning trap uses a strong (7 T) uniform magnetic field generated by a superconducting solenoid to confine charged particles radially via the Lorentz force. Along the bore axis, an electric potential well is generated by large-diameter cylindrical electrodes to confine the charged particles axially. The $\beta$-decay products experience negligible distortions to their momenta upon leaving the trap since energy shifts induced by the shallow electric potential are negligible compared to their kinetic energies. Furthermore, by placing detectors on either end of the Penning trap, TAMUTRAP will have $4\pi$ collection of the daughter $\beta$ and proton products given its uniquely-large inner diameter of 180 mm. A recent summary of the TAMUTRAP facility is discussed in Refs. [1,5].

The light-ion guide (LIG) technique [4,6] will be used to produce the radioactive ion beams (RIBs) of interest to the TAMUTRAP program: $^{20,21}$Mg, $^{24,25}$Si, $^{28,29}$S, $^{32,33}$Ar and $^{36,37}$Ca. This system could be upgraded in the future to charge-breed and inject in the K500 cyclotron for re-accelerated RIBs, as well as to provide a new dedicated general purpose decay station.

Fig. 1 shows the planned layout of the system at the Cyclotron Institute. A high-intensity $^{3}$He from the K150 cyclotron will impinge on a target in the LIG chamber. The reaction products will be stopped in a gas cell and guided to a nozzle by a continuous flow of ultra-high purity helium, whereupon they will enter a sextupole ion guide (SPIG) system. The ions will be transported through apertures for differential pumping before being accelerated up to 65 keV for transport through LSTAR. The entrance of a radiofrequency quadrupole (RFQ) Paul trap will be placed at the image of LSTAR. This device will collect, cool and bunch the purified RIB before being transported up to the TAMUTRAP station above the shielding blocks.

In order to avoid overloading the RFQ with contaminant ions, impurities of nearby masses must be removed using an effective isobar

* Corresponding author.
*E-mail address:* gberg@nd.edu (G.P.A. Berg).

https://doi.org/10.1016/j.nima.2024.169944
Received 27 March 2024; Received in revised form 27 September 2024; Accepted 28 September 2024
Available online 5 October 2024
0168-9002/© 2024 Elsevier B.V. All rights are reserved, including those for text and data mining, AI training, and similar technologies.

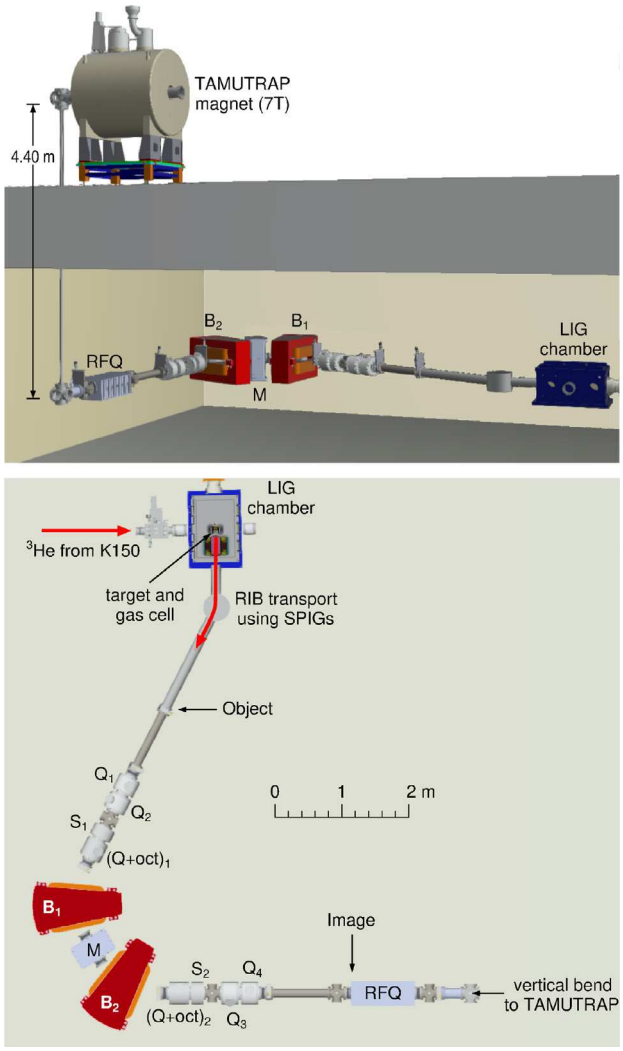


**Fig. 1.** Layout of the LSTAR isobar separator at the Cyclotron Institute in relation to the LIG chamber for RIB production and the RFQ at the focal plane to collect the purified beam. Lower panel: top view showing the dispersive plane. Upper panel: side view with the TAMUTRAP magnet sitting atop shielding blocks. The annotations are defined in the text.

separator. To that end, we have designed the isobar-separator LSTAR with sufficiently high mass separation and a high transmission of 95% for the desired RIB. Such a system was developed and is operated at the CARIBU facility of Argonne National Laboratory, see Ref. [7]. We used this system as guidance to design LSTAR.

The isobar separator at CARIBU demonstrates that high mass separation can be achieved using a combination of electrostatic multipoles and magnetic dipoles. We adopted the same general design. We also use electrostatic focusing and higher-order elements, so that most of the separator settings are independent of mass at a given ion energy. In addition, like in CARIBU, LSTAR is symmetric relative to the center of the system in first order. However, we modified the field settings and broke the symmetry in higher order to optimize the mass resolution. Moreover, the ion-optical tune of our system, shown in Fig. 2, is different from the CARIBU isobar separator.

The following section summarizes the design considerations and requirements, given by the physics goals and the physical constraints of the laboratory space. Section 3 describes the layout of LSTAR followed by a detailed presentation of the ion-optical design. Brief descriptions of the magnetic and electrostatic elements are given in Section 5. The expected performance on the basis of a Monte-Carlo simulation is summarized in Section 6, followed by a conclusion in Section 7.

## 2. Design considerations and requirements

The design of LSTAR is constrained by the science goals of the project and by the properties of the incoming RIB. Results from the simulations of the RIB delivery system are discussed in the introduction of Section 6. The design was guided by the following list of initial conditions:

1. Horizontal and vertical RMS object sizes of less than ±0.5 mm at the object location to account for 99% in the incoming RIB.
2. Horizontal and vertical RMS divergences of up to ±0.5 mrad at the object location to account for 99% in the incoming RIB.
3. A kinetic energy spread of the incoming beam of less than ±3.3 eV ($\pm 1\sigma$) at a maximum energy of 65 keV.

The science-driven requirements for LSTAR are presented in the list below. The system must be able to select ions with mass up to $A = 50$, at charge state $Q = 1$, with a high transmission and minimal contamination. This is why the optimization procedure, that relies on a subset of the whole phase space of interest, aimed for the mass resolving power to be larger than 16,500 and the mass resolution to be larger than 7,000. Finally, the image must meet the requirements of the transport line that delivers the purified RIB to TAMUTRAP.

1. Separation of masses with $M/\Delta M \geq 3000$ validated with the Monte Carlo procedure described in Section 6.
2. Transmission >95%.
3. LSTAR will allow the analysis of particles with masses up to $A = 50$, at charge state $Q = 1$.
4. A compact layout to fit within the limited space available.
5. A horizontal waist at the exit (Image) of LSTAR.
6. An image that is less than ±3 mm in the vertical and horizontal directions.
7. An image with minimal divergence in both directions.

In the LSTAR design we defined the mass resolving power, $R_m$, of a focusing electromagnetic system (*i.e.* with $(x|a) = 0$) by the mass dispersion $(x|dm/m)$ divided by the magnification $(x|x)$ and the full object size $2x_0$ at the entrance of LSTAR as follows:

$$R_m = \frac{(x|dm/m)}{(x|x)2x_0}. \tag{1}$$

The mass resolution, a quantity introduced as a figure of merit to optimize the system, is determined by replacing the denominator $(x|x)2x_0$ in Eq. (1), by the maximum difference $x_{\mathrm{HO}} = x_{\max} - x_{\min}$ of 189 characteristic rays (defined later in the text).

The design mass resolving power $R_m$ is achieved by a system of two dipoles bending both through an angle of 62.5° in the same direction with appropriate optical tunes to provide a high mass dispersion.

In a realistic system the higher-order aberrations will limit the mass separation actually achievable. In this case the image size $(x|x)2x_0$ at the focal plane has to be replaced by the image size $x_{\mathrm{HO}}$ including HO effects. The best approach to minimize $x_{\mathrm{HO}}$ would have been to perform Monte Carlo calculations with many rays. Such calculations, however, are time consuming. Therefore, we defined 189 "characteristic rays" distributed in a grid-like pattern within the acceptances of the system as defined in Ref. [7]. These characteristic rays serve solely as a guiding tool within the optimization procedure. In the case of LSTAR, the angle acceptances are 5 mrad in both the $x$ and $y$ direction, while the energy spread is 3.3 keV. The accepted object sizes are 0.5 mm in both horizontal and vertical directions. We defined the image size as the horizontal extent of those rays at the focal plane in order to achieve the best resolution by fitting the HO parameters of the system. The ion optical parameters resulting from the optimization of the mass resolving power was then verified using the final HO ion optical transfer matrix in Monte Carlo calculations with 1500 rays as described in Section 6. This procedure, used to successfully optimize the mass

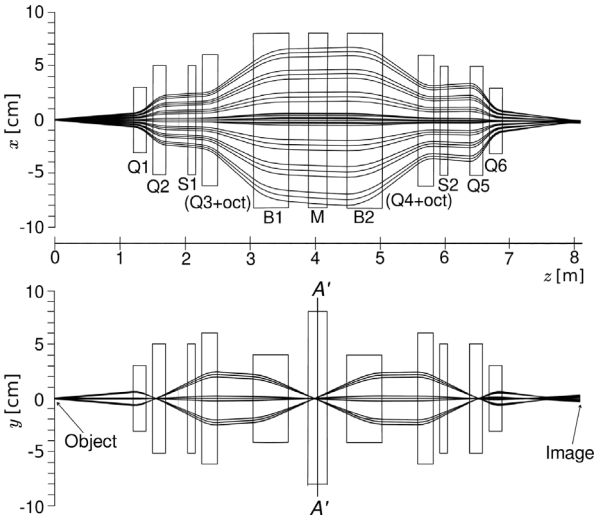


**Fig. 2.** Third order ion optics in the dispersive (top) and non-dispersive (bottom) planes. The rays shown correspond to the 189 characteristic rays defined in the text.

resolution of the magnet separator SECAR, is discussed in more detail in Ref. [8].

The ion-optical code COSY INFINITY [9] and the notations and definitions therein were used in this study to develop and optimize the ion-optics of LSTAR. A detailed discussion of the ion-optical design will be given in Section 4.

## 3. Layout

The layout of the LSTAR isobar separator is shown in Fig. 1. The beam enters the separator at the Object point with sizes of ±0.5 mm in $x$ and $y$ directions. The angle acceptances are ±5 mrad as listed under conditions item 2 in Section 2. LSTAR starts with a 1.2-m-long drift from the Object to the entrance (effective field boundary) of the first quadrupole $Q_1$. The complete LSTAR system consists of nine electrostatic elements ($Q_1$, $Q_2$, $S_1$, $(Q+oct)_1$, M, $(Q+oct)_2$, $S_2$, $Q_3$, $Q_4$), and two magnetic dipoles ($B_1$ and $B_2$). The electrostatic elements are labeled Q (quadrupoles), S (sextupoles), (Q+oct) (quadrupole plus octupole) and a multipole M, which functions as a combined quadrupole, sextupole and octupole, and follows a so-called "squirrel cage" design as shown in Ref. [7]. Extensive ion-optical calculations were conducted to meet the requirements. The resulting design parameters and the dimensions of the layout are listed in Table 1. The elements are mirror symmetric about the center of M so that $Q_1 = Q_4$, $Q_2 = Q_3$, etc. However, in the optimization to achieve the highest mass separation, the field settings of identical elements, including the higher order elements, are slightly different.

The concept and layout of LSTAR was inspired by the design of Ref. [7]. However, the layout was modified to accommodate the design goals. The space requirements of this project are discussed and shown in Fig. 2 of Ref. [10].

## 4. Design and ion optics

The ion-optical design is shown in Fig. 2. In the upper panel, characteristic rays are shown in the dispersive $x$ (horizontal) plane. The lower panel shows the rays in the non-dispersive $y$ (vertical) plane. The characteristic rays include rays with maximum extent in both planes and define, therefore, the required good field regions. The rectangular sizes for each element represent the effective field length in the $z$ (beam-axis) direction and the good-field region in the transverse directions.

**Table 1**
The longitudinal lengths and aperture radii of the elements of the isobar separator system LSTAR as entered in the COSY INFINITY input file.

| Element | | Properties | |
|---|---|---|---|
| Notation | Description | Effective length [m] | Aperture radius [mm] |
| DL1 | drift length | 1.20 | |
| $Q_1$ | quad | 0.20 | 30 |
| DL2 | drift length | 0.10 | |
| $Q_2$ | quad | 0.20 | 50 |
| DL3 | drift length | 0.34 | |
| $S_1$ | hexapole | 0.12 | 50 |
| DL4 | drift length | 0.10 | |
| $(Q+oct)_1$ | quad+octupole | 0.24 | 60 |
| DL5 | drift length | 0.548 | |
| $B_1$ | dipole | 0.54542[a] | |
| DL6 | drift length | 0.30 | |
| *M* | multipole | 0.30 | 80 |
| DL7 | drift length | 0.30 | |
| $B_2$ | dipole | 0.54542[a] | |
| DL8 | drift length | 0.548 | |
| $(Q+oct)_2$ | quad+octupole | 0.24 | 60 |
| DL9 | drift length | 0.10 | |
| $S_2$ | hexapole | 0.12 | 50 |
| DL10 | drift length | 0.14 | |
| $Q_3$ | quad | 0.20 | 50 |
| DL13 | drift length | 0.10 | |
| $Q_4$ | quad | 0.20 | 30 |
| DL12 | drift length | 1.20 | |

[a] These dipole values were calculated from COSY NFINITY.

**Table 2**
First-order transfer matrix elements of the complete LSTAR system from Object to Image.

| Matrix element | Name | Magnitude |
|---|---|---|
| $(x\|x)$ | $x$ magnification | −0.556 |
| $(x\|a)$ | $x$ focus | 0.119 m/rad |
| $(x\|dm/m)$ | mass dispersion | 9.38 m |
| $(y\|y)$ | $y$ magnification | 1.04 |
| $(y\|b)$ | $y$ focus | 0.04 m/rad |

To first order, the ion-optical design is mirror symmetric about the center (*i.e.* the plane $A$-$A'$ of electrostatic element $M$ as shown in Fig. 2) in order to keep higher order aberrations small. Deviations from perfect symmetry are the result of empirical optimization for maximum resolution. The mass resolution is increased by 10% after deviation from symmetry.

The first-order transfer matrix elements from Object to Image are shown in Table 2. The total image size in the $y$ direction is 1.2 mm, mainly owing to a 3rd-order aberration which was not minimized for the smallest size in order to obtain a higher resolution.

In order to achieve symmetry about the center $A$-$A'$ of LSTAR shown in Fig. 2, the transfer matrices from Object to $A$-$A'$ were initially tuned for $(y|b) = 0$ and $(a|a) = 0$. Owing to the asymmetry introduced to maximize the mass resolution, the matrix elements were changed to $(y|b) = 0.265$ and $(a|a) = 0.488$.

In Fig. 2, the deviation from perfect symmetry can be seen in the upper panel showing different envelopes through $Q_2$ and $Q_5$. Also, the rays through $M$ are not perfectly parallel. In the lower panel, the rays are out of focus in the image location. These deviations from symmetry improve the more important mass resolution at the expense of less critical symmetry.

In first order, the system is slightly underfocused horizontally at the image location (see $(x|a) = 0.119$ in Table 2) to improve the mass resolution. Despite the $(x|a)$ term being non-zero at this location, we apply Eq. (1) and obtain a mass resolving power of $R_m = 16{,}870$. Due to residual higher-order aberrations after sextupole ($S_1$, $S_2$) and octupole (oct) optimization, the final mass resolution is approximately 7,000.

**Table 3**
Specifications for the dipole magnets of LSTAR.

| Quantity | $B_1$ | $B_2$ |
|---|---|---|
| Bending radius, $\rho$ | 0.5 | 0.5 m |
| Max. rigidity, $B\rho$ | 0.26 | 0.26 Tm |
| Max. mag. field, $B_{max}$ | 0.52 | 0.52 T |
| Bending angle | 62.5° | 62.5° |
| Central ray length | 0.54542 | 0.54542 m |
| Vertical gap | 0.08 | 0.08 m |
| Good-field region, GFR | 0.16 | 0.16 m |
| Entrance parameters | | |
| $a$ | 0.43036 | 0.43036 $m^{-1}$ |
| $b$ | −0.0839 | 0.8240 $m^{-2}$ |
| $c$ | 3.770 | 0.9511 $m^{-3}$ |
| Exit parameters | | |
| $a'$ | 0.43036 | 0.43036 $m^{-1}$ |
| $b'$ | 0.1702 | −1.011 $m^{-2}$ |
| $c'$ | 0.0223 | 2.575 $m^{-3}$ |

We will show in Section 6 that this mass resolution leads to an effective separation of $M/\Delta M = 3000$ using a more realistic Monte Carlo simulation of the incoming beam.

The system from Object to Image is optimized up to order 3 in part by shaping the entrance and exit edges of both dipoles and by variable multipoles. The calculation shown in Fig. 2 is performed up to order 3. Calculations up to order 7 were performed and confirmed that orders higher than order 3 are not affecting the ion optics, in particular the critical mass resolution.

## 5. Design of magnetic and electrostatic elements

The electrostatic and magnetic elements of LSTAR will allow to analyze particle masses up to $A = 50$, with a charge state of $Q = 1$, and a maximum energy of 65 keV. This results in a maximum rigidity of $B\rho = 0.243$ Tm. Magnetic fields will be scaled proportionally to the magnetic rigidity of the selected particles, while the electrostatic strengths will be scaled with their energy. The dipole specifications are summarized in Table 3.

The effective field boundaries at the entrance and exit of the dipole magnet are shaped to first (a), second (b), and third order (c) at the entrance and exit according to:

$$\text{Entrance:}\quad z(x) = ax + bx^2 + cx^3 \tag{2}$$

and

$$\text{Exit:}\quad z(x) = a'x + b'x^2 + c'x^3. \tag{3}$$

This was done to provide vertical focusing and higher-order corrections. These equations follow the notation of COSY INFINITY [9]. The first order coefficients in Eqs. (2) and (3) are the tangents of the edge rotations. For a detailed discussion see Fig. 7 and related text in Ref. [8]. We used the default fringe-field profiles of COSY INFINITY in our present calculations. As the various elements are designed and built, the calculated electric and measured magnetic fringe-field profiles will be used in COSY INFINITY to calculate corrections to the fields required (if necessary) to maintain the intended ion-optical properties.

Electrostatic quadrupoles and sextupoles will be designed by a commercial vendor according to our specifications. They will be custom designed following the concept of using shaped electrodes, similar to commercially available systems. Higher order electrostatic lenses or combination of higher order components will follow the "squirrel cage" concept as shown in Ref. [7].

## 6. Expected performance

SIMION [11] simulations of the stopping and transport through the SPIG predict that the ions will have a 3.3 eV energy spread and an emittance of 1.15 $\pi$ mm mrad at the object location. The positions and momenta of the rays resulting from these SIMION simulations were then used as realistic inputs for the studies of the performance of LSTAR.

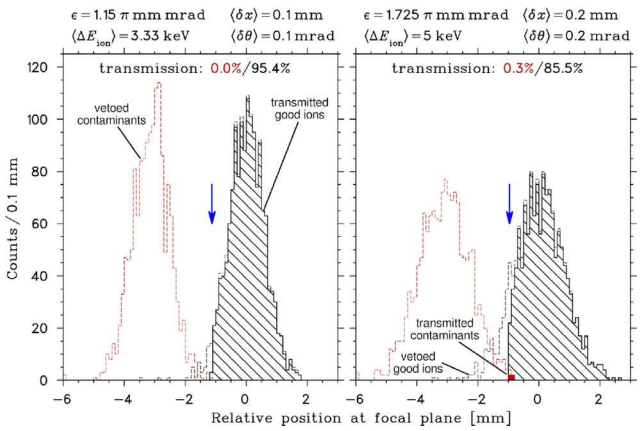


**Fig. 3.** Distributions of good (black) and contaminant ions (red) with $M/\Delta M = 3000$ at the focal plane of LSTAR as calculated using COSY INFINITY [9] with initial ions simulated by SIMION [11]. The hatched distribution centered at zero are the ions of interest, while the red-filled distribution to its left are the contaminant ions that were transmitted through LSTAR. Dashed lines indicate all incident rays, including ones vetoed by the separator and/or the focal plane slits (indicated by the blue arrow). Left: LSTAR is able to fully separate contaminant ions with the expected emittance, energy spread, and reasonable misalignments. Right: even with the emittance and energy spread increased by 50% and misalignments doubled, LSTAR will have >85% transmission with <0.5% contamination.

To understand the sensitivity of LSTAR to the effects of translational and rotational misalignments, we performed a sensitivity study. Transport maps were generated in COSY INFINITY where elements were shifted in $x$ and $y$ in increments of ±100 μm up to ±1 mm, and rotated around $x$ and $y$ by ±100 μrad up to ±1 mrad. Early investigations showed that effects arising from rotations about the beam axis ("roll") are equal to or (more generally) less than the effects of rotations perpendicular to the beam axis. Translational misalignment along the reference axis, within ±1 mm, can be corrected with small changes in the quadrupole fields. A Monte Carlo approach was used to randomly vary the magnitude of the misalignment of each element according to a normal distribution with a 1-$\sigma$ width specified on input; if a randomly-generated misalignment was greater than ±1 mm and/or ±1 mrad, we truncated using the map with the maximum misalignment. Similarly, the predicted energy spread of $\Delta E = 3.3$ eV was randomly included and applied to the 1500 rays produced by the SIMION simulation. These rays were then transported through the randomly-misaligned system ending with the ion distributions at the focal plane of LSTAR. The same misalignments and energy spread were applied for both the ions of interest as well as isomeric contaminants with $M/\Delta M = 3000$.

Examples of the performance studies described above are shown in Fig. 3 where the focal plane distributions of good and contaminant ions are shown. On the left is the 'realistic' situation where the initial rays were taken to be those predicted by SIMION, and the average misalignments applied to the elements were ±0.1 mm and ±0.1 mrad. The plot on the right of Fig. 3 has a 50% larger emittance, 50% more energy spread, and double the spatial/rotational misalignments, representing a more 'pessimistic' scenario of the alignment and incoming beam properties. In both cases, the hatched/filled histograms represent the ions/contaminants which passed through all elements of LSTAR, including a final slit system (blocking the region to the left of the blue arrow). The unfilled dashed histograms represent the position of ions which were stopped in LSTAR and/or by the final slits. As one can see, the 'realistic' simulation completely separates $M/\Delta M = 3000$ contaminants with over 97% transmission efficiency of the ions of interest. Repeated simulations consistently lead to >95% transmission

in the realistic case. Our studies show the energy spread and emittance limit the resolution, with misalignments of the elements only starting to dominate when the 1-$\sigma$ deviations are as large as $\pm$0.5 mm and $\pm$0.5 mrad.

## 7. Conclusion

This article introduces the design and specifications of LSTAR, a crucial component of TAMUTRAP, which is currently under construction at Texas A&M University. LSTAR serves as a mass separator aimed at purifying the RIBs produced using the LIG technique with a $^3$He primary beam. The main function of LSTAR is to prevent overloading TAMUTRAP's RFQ cooler-buncher with unwanted contaminant ions. Once commissioned and operating, LSTAR will be used to transport purified RIB to the existing TAMUTRAP facility, enabling researchers to explore physics beyond the standard model via $\beta$-delayed proton decays using the TAMUTRAP's novel cylindrical Penning trap. In the longer term, future developments may include charge-breeding the RIB from LSTAR using an EBIT [12,13] for re-acceleration using the K500 cyclotron. The performance requirements of LSTAR were rigorously assessed through Monte-Carlo simulations, ensuring its efficacy in the experimental setup.

## Credit authorship contribution statement

**G.P.A Berg:** Writing – original draft, Methodology, Formal analysis, Conceptualization. **D. Melconian:** Writing – review & editing, Supervision, Methodology, Funding acquisition, Formal analysis, Conceptualization. **M. Couder:** Writing – review & editing, Validation. **M. Brodeur:** Writing – review & editing, Methodology, Conceptualization. **V.E. Iacob:** Writing – review & editing, Validation, Investigation. **J. Klimo:** Writing – review & editing, Investigation. **P.D. Shidling:** Writing – review & editing, Validation, Software, Conceptualization.

## Declaration of competing interest

The authors declare that they have no known competing financial interests or personal relationships that could have appeared to influence the work reported in this paper.

## Data availability

Data will be made available on request.

## Acknowledgments

This work was supported by the U.S. Department of Energy, Office of Science, under Award No. DEFG02-93ER40773, and by the Department of Energy, National Nuclear Security Administration, USA under Award No. DE-NA0003841 (CENTAUR). G.P.A.B., M.B., and M.C. acknowledge support of the National Science Foundation, USA under Grants PHY-2011890 and PHY-2310059.

## References

[1] P. Shidling, V. Kolhinen, B. Schroeder, M. Nasser, A. Ozmetin, D. Melconian, TAMUTRAP facility: Penning trap facility for weak interaction studies, Hyperfine Interact. 240 (2019) 40, http://dx.doi.org/10.1007/s10751-019-1584-9.

[2] J.D. Jackson, S.B. Treiman, H.W. Wyld, Possible tests of time reversal invariance in beta decay, Phys. Rev. 106 (1957) 517, http://dx.doi.org/10.1103/PhysRev.106.517, URL https://link.aps.org/doi/10.1103/PhysRev.106.517.

[3] A. Falkowski, M. González-Alonso, O. Naviliat-Cuncic, Comprehensive analysis of beta decays within and beyond the standard model, J. High Energy Phys. 2021 (2021) 126, http://dx.doi.org/10.1007/JHEP04(2021)126, URL https://link.springer.com/article/10.1007/JHEP04(2021)126.

[4] I. Moore, P. Dendooven, J. Ärje, The IGISOL technique–three decades of developments, Hyperfine Interact. 223 (2014) 17, http://dx.doi.org/10.1007/s10751-013-0871-0, URL https://link.springer.com/article/10.1007/s10751-013-0871-0.

[5] P. Shidling, V. Kolhinen, B. Schroeder, M. Nasser, A. Ozmetin, D. Melconian, Ion-trap application: Fundamental weak interaction studies using ion traps, AIP Conf. Proc. 2160 (2019) 070011, http://dx.doi.org/10.1063/1.5127734, URL https://aip.scitation.org/doi/abs/10.1063/1.5127734.

[6] J. Äystö, Development and applications of the IGISOL technique, Nucl. Phys. A 693 (2001) 477, http://dx.doi.org/10.1016/S0375-9474(01)00923-X, Radioactive Nuclear Beams. URL http://www.sciencedirect.com/science/article/pii/S037594740100923X.

[7] C.N. Davids, D. Peterson, A compact high-resolution isobar separator for the CARIBU project, Nucl. Instrum. Methods Phys. Res. Sect. B 266 (2008) 4449, http://dx.doi.org/10.1016/j.nimb.2008.05.148, URL http://www.sciencedirect.com/science/article/pii/S0168583X08007544.

[8] G. Berg, M. Couder, M. Moran, K. Smith, M. Wiescher, H. Schatz, U. Hager, C. Wrede, F. Montes, G. Perdikakis, X. Wu, A. Zeller, M. Smith, D. Bardayan, K. Chipps, S. Pain, J. Blackmon, U. Greife, K. Rehm, R. Janssens, Design of SECAR a recoil mass separator for astrophysical capture reactions with radioactive beams, Nucl. Instrum. Methods Phys. Res. A 877 (2018) 87–103, http://dx.doi.org/10.1016/j.nima.2017.08.048, URL https://www.sciencedirect.com/science/article/pii/S0168900217309488.

[9] K. Makino, M. Berz, COSY INFINITY version 9, Nucl. Instrum. Methods Phys. Res. A 558 (1) (2006) 346–350, http://dx.doi.org/10.1016/j.nima.2005.11.109, Proceedings of the 8th International Computational Accelerator Physics Conference. URL https://www.sciencedirect.com/science/article/pii/S0168900205021522.

[10] D. Melconian, G. Berg, P. Shidling, M. Couder, M. Brodeur, G. Chubarian, V. Iacob, J. Klimo, G. Tabacaru, Expanding RIB capabilities at the cyclotron institute: $^3$He-LIG production with an isobar separator LSTAR, Nucl. Instrum. Methods Phys. Res. B 541 (2023) 99–101, http://dx.doi.org/10.1016/j.nimb.2023.04.043, URL https://www.sciencedirect.com/science/article/pii/S0168583X23001866.

[11] D.A. Dahl, SIMION for the personal computer in reflection, Int. J. Mass Spectrom. 200 (2000) 3, http://dx.doi.org/10.1016/S1387-3806(00)00305-5, URL http://www.sciencedirect.com/science/article/pii/S1387380600003055.

[12] M.A. Levine, R.E. Marrs, J.R. Henderson, D.A. Knapp, M.B. Schneider, The electron beam ion trap: A new instrument for atomic physics measurements, Phys. Scr. 1988 (T22) (1988) 157, http://dx.doi.org/10.1088/0031-8949/1988/T22/024.

[13] R.E. Marrs, S.R. Elliott, D.A. Knapp, Production and trapping of hydrogenlike and bare uranium ions in an electron beam ion trap, Phys. Rev. Lett. 72 (1994) 4082–4085, http://dx.doi.org/10.1103/PhysRevLett.72.4082, URL https://link.aps.org/doi/10.1103/PhysRevLett.72.4082.